Materials Science & Engineering A 683 (2017) 164–171

Contents lists available at ScienceDirect

Materials Science & Engineering A

journal homepage: www.elsevier.com/locate/msea

Influence of thermal treatments on the mechanical properties and the martensitic transformation in Fe-Pd-Mn ferromagnetic shape memory alloy

F.G. Bonifacich[a], J.I. Pérez-Landazábal[b], O.A. Lambri[a,*], P.B. Bozzano[c], V. Sánchez-Alarcos[b], J.A. García[d], G.I. Zelada[a], V. Recarte[b], G.J. Cuello[e]

[a] CONICET-UNR - Laboratorio de Materiales, Escuela de Ingeniería Eléctrica, Centro de Tecnología e Investigación Eléctrica, Facultad de Ciencias Exactas, Ingeniería y Agrimensura. Avda. Pellegrini 250, 2000 Rosario, Argentina
[b] Departamento de Física, Universidad Pública de Navarra. Institute for Advanced Materials (INAMAT), Universidad Pública de Navarra, Campus de Arrosadía, 31006 Pamplona, Spain
[c] Laboratorio de Microscopía Electrónica, Unidad de Actividad Materiales, Centro Atómico Constituyentes, Comisión Nacional de Energía Atómica e Instituto Sábato – Universidad Nacional de San Martín, Avda. Gral. Paz 1499, 1650 San Martín, Argentina
[d] Departamento de Física Aplicada II, Facultad de Ciencias y Tecnología, Universidad del País Vasco. BC Materials (Basque Centre for Materials, Application and Nanostructures), Apdo. 644, 48080 Bilbao, País Vasco, Spain
[e] Institute Laue-Langevin, 71 Av. des Martyrs, B.P. 156, 38042 Grenoble Cedex 9, France

ARTICLE INFO

Keywords:
Fe-Pd-Mn
Ferromagnetic shape memory alloys
Martensitic transformation
Precipitation processes
Hardening
Damping capacity

ABSTRACT

The effects of high temperature thermal treatments on the hardening behaviour, the damping capacity and the martensitic transformation in $Fe_{66.8}Pd_{30.7}Mn_{2.5}$ Ferromagnetic Shape Memory Alloy have been determined by mechanical spectroscopy. Annealing below 753 K, lead to a hardening of the alloy without a marked decrease in the damping capacity. In addition, they increase both the austenite finish transformation temperature and the intensity of the damping peak related to the martensitic transformation. This variation can be controlled by the small volume fraction precipitation of small α phase particles. In contrast, thermal treatments performed above 753 K lead to a further hardening of the alloy, but they decrease the austenitic finish transformation temperature and the intensity of the damping peak related to the martensitic transformation; as a consequence of the decomposition of the metastable γ phase into the $\alpha+\gamma_1$ stable phases. In addition, two new damping peaks related to the mobility of dislocations and grain boundaries have been discovered at around 700 K and 900 K, respectively.

1. Introduction

The face centered tetragonal (fct) martensitic phase in Fe-Pd alloys allows the magnetic shape memory effect by reorientation of martensite variants via twin boundary motion. The fct martensite can be obtained when cooling fcc austenite through the martensitic transition (MT) [1–12]. This structural transformation from fcc to fct only takes place in a very narrow compositional range (29 < at% Pd < 32) and the transformation temperatures lie typically below room temperature (RT) [3,13]. The addition of a new element has been shown to be an effective way to control the transformation characteristics of these alloys [14–22]. For instance, it has been shown that the substitution of 1% of Fe by Mn fully inhibits the irreversible fct-bct transformation without decreasing the fcc-fct transformation temperature, which highly improves the temperature range for the magnetic field induced strain. In addition, the substitution of 2.5% of Fe by Mn highly increases the thermoelastic martensitic transformation temperature [23].

The equilibrium phase diagram of the Fe-Pd system shows at low temperature five distinguishable regions as a function of the atomic Pd content, x, [24]: (i) a bcc-Fe (α-Fe) solution extending to x=1–2% Pd, (ii) the coexistence of α-Fe and equiatomic $L1_0$-FePd (γ_1) up to 50% Pd, (iii) γ_1 for 50 < x < 60, (iv) fcc-$FePd_3$ (γ_2 with Cu_3Au structure for 60 < x < 90, and (v) fcc-FePd (γ) disordered phase for higher Pd content. On the other hand, Fe and Pd form at high temperature a continuous fcc solid solution (γ-FePd) that, suitably quenched to RT, corresponds to the austenite phase. This metastable γ-FePd austenite decomposes on heating according to the phase diagram in α-Fe and fcc-Fe-Pd (γ_1) phase. A large amount of internal stresses, point defects, dislocations and other bi- and tri-dimensional microstructural defects are also expected to be retained in the quenching process. Those defects may also play an important role in the characteristics of the MT and the

* Corresponding author.
E-mail address: olambri@fceia.unr.edu.ar (O.A. Lambri).

http://dx.doi.org/10.1016/j.msea.2016.12.012
Received 29 September 2016; Received in revised form 27 November 2016; Accepted 1 December 2016
Available online 02 December 2016
0921-5093/ © 2016 Elsevier B.V. All rights reserved.

relative stability of the structural phases [25–34]. For instance, the large misfit between the cell parameters of fct and bct martensites point out to a critical role of dislocations in the accommodation of these phases [26].

The aim of the current research is to analyze by mechanical spectroscopy the impact of thermal treatments between RT and 1000 K on both the mechanical properties and the MT in a Fe-30.7at %Pd-2.5at%Mn alloy. Indeed, mechanical spectroscopy is a very sensitive and non-destructive characterization technique widely used in materials science to study the defects interaction processes, their effects on the hardening and damping [35–38] and the martensitic transformation phenomenon [35,39–43]. In addition, other characterization techniques as, differential scanning calorimetry, X-ray diffraction and neutron diffraction, were also used. The performed experiments allow to determine the appropriated thermal treatments necessary to improve the mechanical properties, the damping capacity and the transformation temperature range of the MT. Besides, new relaxation peaks have been identified and correlated to specific microstructural mechanisms. Finally, the decomposition of the austenitic phase at high temperatures has been studied to control the degradation of the martensitic transformation.

2. Experimental

Polycrystalline ingots of nominal composition Fe-30.7at%Pd-2.5at %Mn were prepared from high purity elements by arc melting under protective Ar atmosphere (called hereafter FePdMn). The ingots were homogenized in vacuum quartz ampoules at 1273 K during 24 h. In order to retain the disordered γ (Fe, Pd) cubic structure in which the MT occurs, the ingots were subjected to a 30 min annealing treatment at 1173 K in a vertical furnace followed by quenching into iced water (AQ). Once treated, the composition of the elaborated alloys was analyzed by energy dispersive X-ray spectroscopy (EDS) in a Jeol JSM-5610LV Scanning Electron Microscope. The alloy shows a martenstitic start temperature, M_s=315 K and martensitic finish temperature, M_f =285 K. The alloy is always kept above 250 K to avoid the formation of the irreversible martensitic phase.

Scanning electron microscopy (SEM) images of FePdMn alloy thermally treated at several temperatures were performed under vacuum in a FEI Quanta 200 scanning electron microscope operated at 20 kV and supplied with an EDS Apollo device. The backscattered electrons images obtained at RT does not shows the twin variant band morphology characteristic of the fct martensitic phase.

Differential Scanning Calorimetry (DSC) measurements were carried out at a heating/cooling rate of 10 K/min in a TA Q100 calorimeter under nitrogen protective atmosphere.

A BRUKER (axs) D8-Advance powder diffractometer with a high temperature chamber was used to obtain X-ray diffraction (XRD) patterns under high vacuum. The Cu K_α radiation was used as incident radiation and the tube working conditions were 30 kV and 20 mA. Neutron thermodiffraction studies were performed at the D20 powder diffractometer under vacuum (10^{-2} Pa) from RT up to 1000 K at a heating rate of 4°/minute in the Laue-Langevin Institute, Grenoble, France. The neutron wavelength was 1.3 Å.

Mechanical spectroscopy (MS) studies, which often involves the simultaneous measurement of damping (internal friction, Q^{-1}) and the natural resonance frequency (f, f^2 being proportional to the elastic shear modulus), as a function of temperature were performed in an inverted torsion pendulum working at around 1 Hz under Ar at atmospheric pressure. The maximum strain on the sample surface was 5×10^{-5}. The heating and cooling rates employed in the tests were 1 K/minute. A heating run and its following cooling run is called a thermal cycle. The starting temperature of the measurements is 250 K in order to avoid the formation of the irreversible martensitic transformation. During the successive thermal cycles in the cooling part at temperature below 350 K, the recording of data was stopped due to the loss of linearity for the cooling-down ramp.

Amplitude dependent damping (ADD), i.e. damping as a function of the maximum strain on the sample, ε_0, was calculated from Eq. (1) [38,44,45].

$$Q^{-1}(\varepsilon_0) = -\frac{1}{\pi}\frac{d\,(\ln(A_n))}{dn} \quad (1)$$

where A_n is the area of the n^{th} decaying sinusoidal oscillation and n is the period number. The decaying of the oscillations were performed at constant temperature (T ± 0.5 K) and polynomials were used to analyze the curves by Chi-square fitting. Subsequently the Eq. (1) was applied. Polynomials of degree higher than 1 indicate that Q^{-1} is a function of ε_0 leading to the appearance of ADD effects, as it can be inferred easily. This procedure allows to obtain damping as a function of the maximum strain on the sample (ε_0) from free decaying oscillations [38,44,45]. The strength of the ADD can be determined through the average slope of the $Q^{-1}(\varepsilon_0)$ curve using the S coefficient [38,39,44,45]:

$$S = \frac{\Delta Q^{-1}}{\Delta\varepsilon_0} \quad (2)$$

where ΔQ^{-1} is the damping change corresponding to the full amplitude changes $\Delta\varepsilon_0$ measured in the whole oscillating strain range. Depending both on the oscillating strain level (usually higher than 10^{-6}) and on the measuring temperature, the damping can be either amplitude independent or amplitude dependent.

3. Results and discussion

Fig. 1 show the temperature dependence of the damping and elastic shear modulus for the as-quenched sample during the first thermal cycle. The initial temperature is well below M_f, so the measurements start in martensitic phase. In order to better see the different processes, Fig. 1.a shows the low temperature range (250–600 K) and Fig. 1.b the high temperature range (600–1000 K). Several damping peaks can be observed at around 300 K, 425 K, 700 K and 900 K. The first peak at 300 K measured during warming (absent during the cooling run) is related to the reverse MT, in agreement with previous works [22,23,39,41]. The non appearance of the MT peak during cooling is indicating clearly that changes in the microstructure occur during the heating up to 1000 K.

The P_1 peak at 425 K reduces its height during the cooling as a consequence of the recovery of the structure (see Fig. 1.a) [39,41]. Previous works in $Fe_{70}Pd_{30}$, $Fe_{67}Pd_{30}Co_3$ and $Fe_{66.8}Pd_{30.7}Mn_{2.5}$ have demonstrated that the mechanism responsible of P_1 peak is a dislocation dragging process controlled by the migration of vacancies without break away [39,41].

The third peak, the so called P_2 peak in Fig. 1.b at around 700 K is evident after the background damping subtraction, see Fig. 2.a. Damping background subtraction was made by means of Peak Fit V.4 software [46] using cubic polynomials. The peak height decreases during cooling (empty circles) and its height is restored after in situ plastic torsion deformation (triangles), so the physical mechanism controlling this peak could be related to dislocations [35,36,47]. Moreover, the influence of a bias stress of 5×10^{-5} superimposed to the measuring stress has been investigated for the plastically deformed state of the sample. Clear changes of damping cannot be detected when the bias stress is applied (Bias On, see full triangles in Fig. 2a).

The activation energy, H_{P2}, and pre-exponential factor, τ_{0P2}, of the relaxation time controlling P_2 peak were determined from an Arrhenius plot (the shift of the peak temperature due to a shift in the oscillating frequency), Fig. 2b. The activation energy and pre-exponential factor equal H_{P2}=(165 ± 15) kJ/mol and $\tau_{0\text{-}P2}=4\times10^{-(14.0\pm0.5)}$ s, respectively.

The appearance of a damping peak in cold worked austenitic steels is well known to occur at around 600 K and with an activation energy value close to the diffusion of carbon in γ-Fe (115 kJ/mol) [48–50]. This damping peak can be related to the interaction of dislocation with

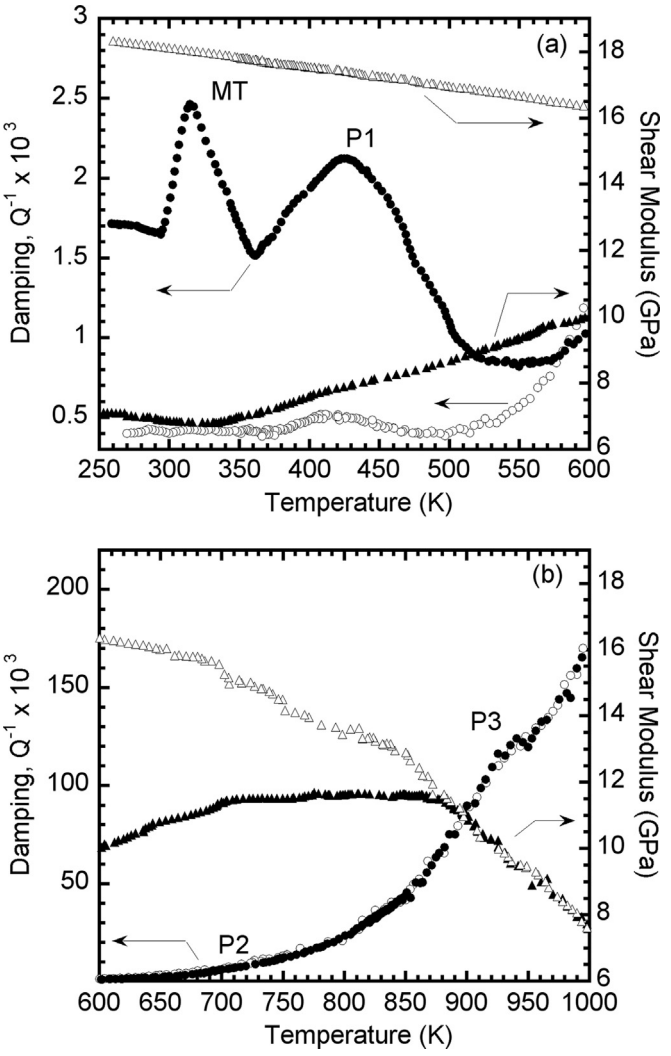

Fig. 1. Damping (circles) and elastic shear modulus (triangles) for a $Fe_{66.8}Pd_{30.7}Mn_{2.5}$ alloy. Full symbols: warming. Empty symbols: cooling. (a) low temperature zone between 250 K and 600 K. (b) high temperature zone between 600 K and 1000 K.

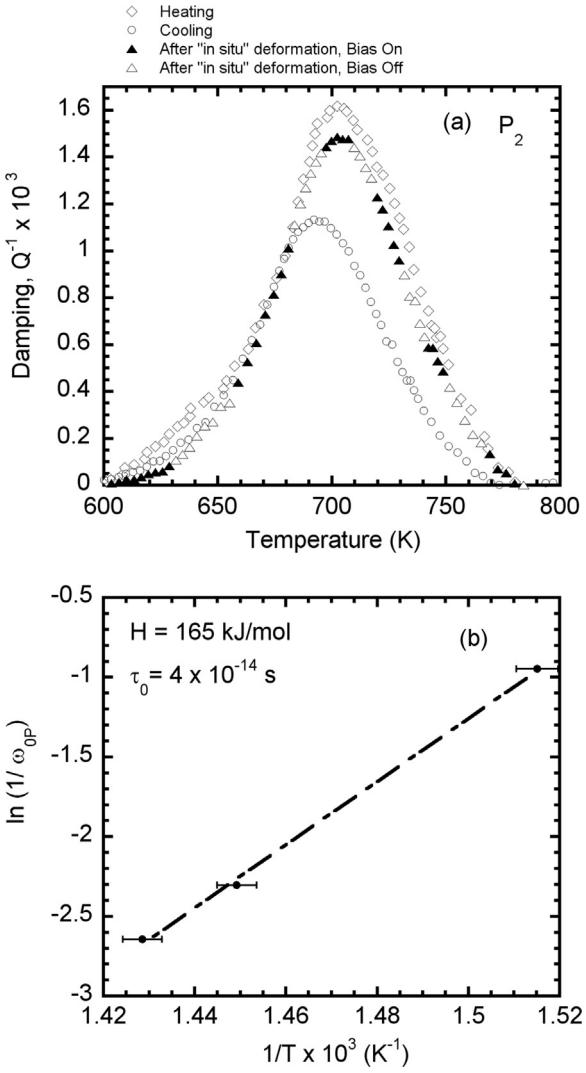

Fig. 2. (a) P_2 peak after background subtraction. The influence of a 5×10^{-5} bias stress superimposed to the measuring oscillating stress on the P_2 damping peak for the sample after deformation in situ is shown. (b) Arrhenius plot corresponding to P2 peak.

solute atoms according to the Schoeck model for the cold work peak, but obviously with solutes atoms in a fcc lattice [51]. However, the P_2 peak in the present work exhibits higher peak temperature and activation energy than the cold work peak in γ-Fe. Moreover, the development of a cold work peak must be related to the development of the Snoek relaxation peak [35,51]. The relaxation peak due to the mobility of carbon atoms in γ-Fe, which appears at around 500 K, was not detected in the present work; as it can be inferred from Fig. 1. In γ-Fe the damping peak related to the mobility of carbon atoms in the fcc lattice is not related to the jump of isolated atoms from an octahedral/tetrahedral site to another [35,36], instead it is related to the movement of atoms pairs interstitial-substitutional or interstitial-interstitial [52,53]. Therefore, a relation of P_2 peak with the Schoeck's cold work peak should be diminished.

In addition, the non appearance of the peak related to the mobility of carbon atoms in the fcc lattice, also diminishes the possibility of relating P_2 with a Snoek-Koester (SK) type damping peak [35,54]. In addition, for this case, the activation energy which should be expected for the SK would result smaller than the value measured for P_2 peak [35,54].

On the other hand, within the so called medium temperature range (0.3 Tm – 0.7 Tm, Tm being the melting temperature), the damping relaxation processes can be controlled by both: (i) the cross slip of dislocations between different slip planes and (ii) the gliding of dislocations controlled by the jog climbing [35]. In fact, the peak temperature for P_2 peak corresponds to around 0.4 Tm and then, it is well inside the medium temperature range. However, we can eliminate a mechanism involving cross slip of dislocations between different slip planes since the bias stress superimposed on the oscillating stress does not lead to clear changes in the damping values of P_2 peak, see Fig. 2. Indeed, full triangles (Bias On) and empty triangles (Bias Off) describe a continuous line for P_2 peak without differences between them, i.e. the same peak with Bias-On and –Off is obtained [55].

The peak temperature for P_2 is above the temperature for vacancy migration, so, this suggests that a vacancy–dislocation interaction would be responsible for the relaxation. Indeed, in electron irradiated high purity α-iron, the recovery of the excess of vacancies promoted by the irradiation is finished at temperatures above 600 K [56]. In addition, for Fe–10 at% Si, the recovery of the quenched-in-vacancies develops up to around 700 K [57].

The self diffusion energy in metals, H_{sd}, can be written as the sum of the formation energy, H_{vf}, and migration energy, H_{vm}, of vacancies [58,59]. If the diffusion process is of type pipe diffusion, i.e. diffusion along the dislocation line, the activation energy, H_d, is related to H_{sd} through $H_d = c \cdot H_{sd}$, where "c" has values between 0.6 and 0.8, depending on the type of dislocation core [47,58,60]. In iron the reported values for H_{sd} are close to 298 kJ/mol [61,62] and assuming c=0.6

[47,59,60], it leads to H_d values close to 178 kJ/mol; which is in a reasonable agreement with the values of the activation energy measured for P_2 peak. Therefore, the physical mechanism controlling P_2 could be related to the process detailed in (ii), i.e. the vacancies are created and dragged by the dislocation movement. In fact, this mechanism has been already reported to appear at around 1000 K (≈0.4 Tm) in molybdenum [60], which has a higher melting temperature (2896 K) than iron (1538 K). Moreover, the peak temperatures for the peak recorded in molybdenum and P_2 correspond in both cases to around 0.4 Tm of each correspondent metal. In addition, the pre-exponential factor of the relaxation time for the peak recorded in molybdenum is 1×10^{-14}[60,63], which results also in agreement with the value measured for P_2. Consequently, P_2 peak could be related to the formation and diffusion of vacancies assisted by the dislocation movement [60].

Finally, the peak at around 900 K, called P_3, exhibits an activation energy H_{P3}=230 kJ/mol, determined from an Arrhenius plot. The calculated activation energy and the peak temperature allow to correlate easily this peak to the solute grain boundary peak of palladium in iron [35,64]. In fact, in polycrystalline pure metals the grain boundary sliding leads to the appearance of a grain boundary peak (solvent peak) with an activation energy close to self diffusion one. The alloying elements lead to both a decrease in the peak height of the solvent peak and to the appearance of another grain boundary peak, at higher temperature and with higher activation energy, called the solute grain boundary peak. Depending on the concentration of solute atoms both peaks could be observed [35,64–66]. In the present case the solvent grain boundary (at around 800 K in iron) could not be detected due to the large solute concentration [35,64–68]. Besides this, a clear change of P_3 during the cooling run cannot be detected.

On the other hand, the effect of temperature on the elastic shear modulus is also shown in Fig. 1 (right axis). During warming, there is a slope change in the shear modulus curve (G) linked to the reverse MT peak in the temperature region between 300 and 350 K. At higher temperatures, the shear modulus increases to a maximum value at around 773 K and then it decreases. On cooling the shear modulus increases and below around 673 K it keeps nearly constant. The non appearance of the jump-down in the modulus curve on the cooling ramp (direct MT) is promoted by the precipitation that takes place at 1000 K that inhibits the MT (this point will be discussed in the following paragraphs).

The first anomalous behaviour of the modulus, i.e. the increase in modulus as the temperature increases, up to around 573 K (see Fig. 1.a), was related to the dragging of point defects by dislocations without break-away [39,41].

Above 673 K the recovery of defects changes the shape of the modulus in $Fe_{70}Pd_{30}$ alloys [39,41]. Then, a straightforward analysis allows to correlate the behaviour of the modulus in FePdMn alloys above 673 K with a recovery of the microstructure. Besides, the marked decrease above 900 K is related to the increase in the grain boundary mobility, revealed by appearance of the P_3 peak, and a further recovery of the structure. In addition, the whole behaviour of the modulus curves during the thermal cycle involves a 90% increase during cooling and could be also related to the appearance of a precipitation process overlapped to the microstructural recovery [35,36,65,66].

The behaviour of the dislocation dynamics as a function of temperature in the as-quench FePdMn alloy is revealed through the temperature dependence of the S parameter, Fig. 3 (diamonds, left axis). The S values remain null up to temperatures close to 680 K. At higher temperatures, the S values start to increase and the appearance of ADD behaviour indicates that a break-away process of dislocations from weak pinning points starts above 680 K. In fact, the development of fine precipitates can promote weak pinning points for the thermal assisted break-away of the dislocations, giving rise to the appearance of ADD [35,36,47,58]. Moreover, the development of P_2 peak, see Fig. 2.a, confirms the development of the dislocation movement. In addition, S

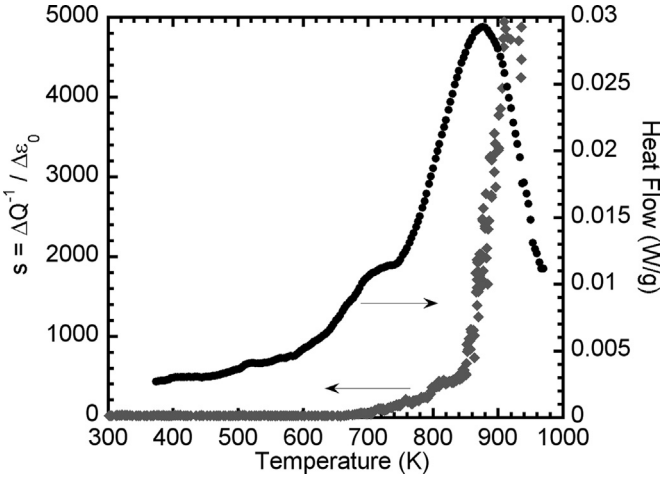

Fig. 3. S parameter (Eq. (2)) measured during warming for as-quench $Fe_{66.8}Pd_{30.7}Mn_{2.5}$ alloy (diamonds). DSC thermogram measured during warming for as-quench $Fe_{66.8}Pd_{30.7}Mn_{2.5}$ alloy (circles).

describes another stage of increase with a different slope above 840 K which should be related either to a modification of the characteristics of the precipitation behaviour or to the development of another precipitation process. DSC thermograms show two exothermic peaks at around 700 K and 873 K, see circles in Fig. 3. The low temperature peak overlaps the second one, which shows a much higher enthalpy. It should be stressed the good agreement between the temperatures where S changes its slope and both exothermic reactions. Consequently, a double precipitation process should be expected.

In order to identify the precipitation stages, X-ray and neutron diffraction experiments were performed. Fig. 4 shows the XRD spectra recorded at RT in FePdMn after three hours at different annealing temperatures. Only the γ disordered phase (fcc) is present in the alloy in the as-quenched state, see reflections at 42.1° and 48.7°. As the annealing temperature increases, the precipitation of α phase appears as a small reflection at around 43.5°. The peak reflection is wide, so the size of the precipitates must be at the nanometric scale. Finally, the alloy partially decomposed into α and γ_1 phases [69] after annealing at 773 K. This decomposition sequence occurs following the TTT curves [70] in agreement with the stable Fe-Pd phase diagram [69]. The same precipitation sequence measured by neutron thermodiffraction studies

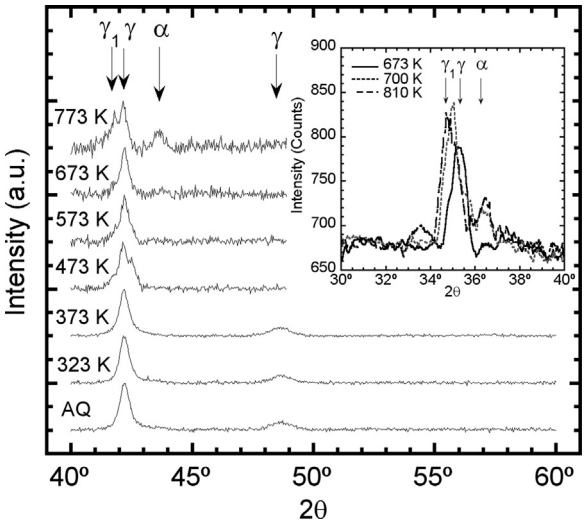

Fig. 4. X-ray diffraction patterns (λ=1.54 Å) recorded at room temperature for different annealing temperatures in $Fe_{66.8}Pd_{30.7}Mn_{2.5}$ alloy (see explanation in the text). Inset: Neutron diffraction patterns (λ=1.3 Å) measured at different temperatures during warming "in situ" at D20.

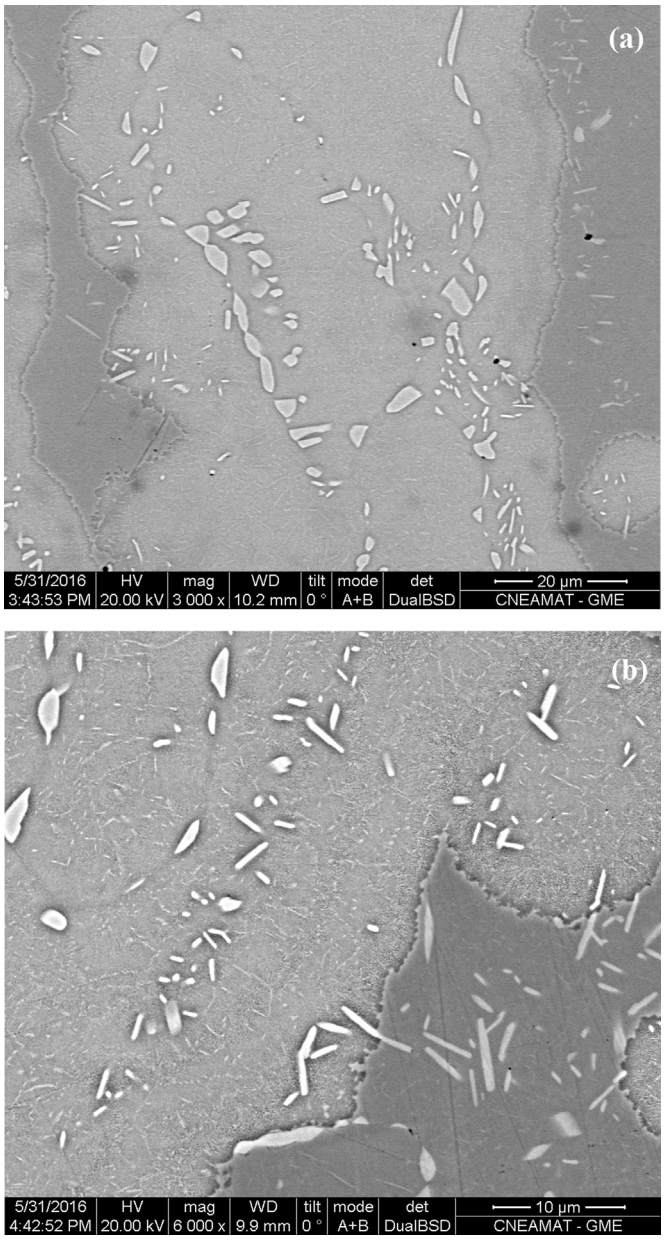

Fig. 5. SEM images corresponding to the $Fe_{66.8}Pd_{30.7}Mn_{2.5}$ alloy thermally treated at 773 K with different magnification.

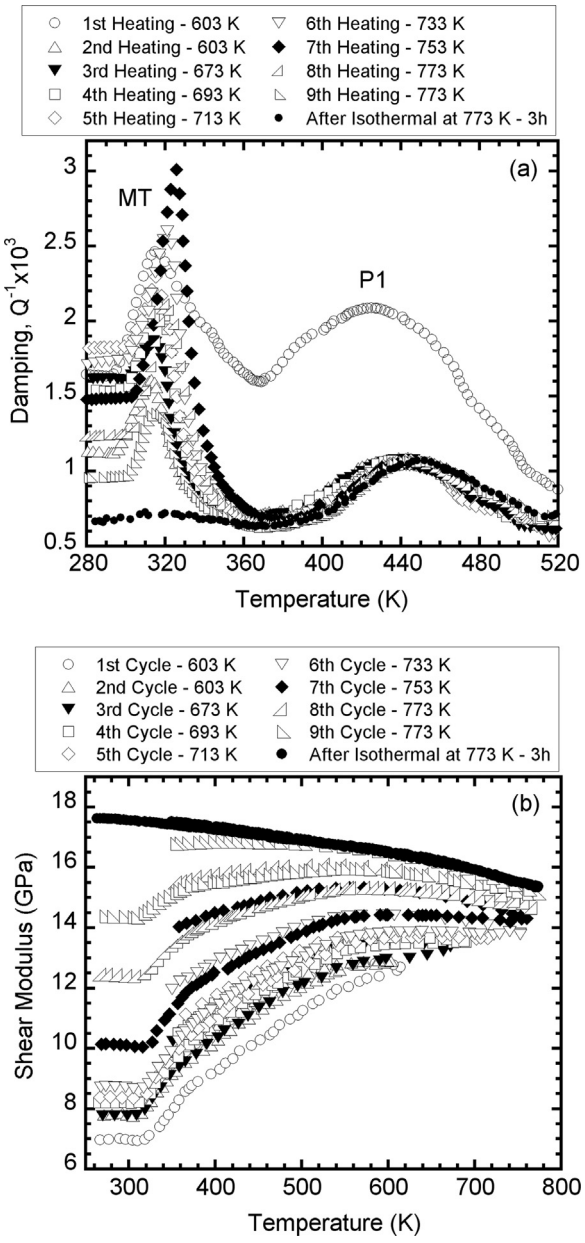

Fig. 6. (a) Damping spectra measured during successive warming runs up to different maximum temperatures. (b) Shear modulus corresponding to curves plotted in (a).

is shown in the inset in Fig. 4. Curves recorded below 673 K exhibit only the γ phase, see full line. On increasing the temperature, the precipitation of the α phase starts; see peak at around 36.5° (dashed line). At higher temperature, the γ phase decomposes in $\alpha+\gamma_1$; see alt-dashed line.

SEM micrographs cannot detect any decomposition process in FePdMn samples annealed below 773 K probably due to the nanometric size of the α particles. In contrast, the FePdMn sample annealed at 773 K shows new phases in the form of needle shaped precipitates in agreement with the above results, see Figs. 5a and 5b.

Therefore, the first exothermic peak at low temperatures observed by DSC in Fig. 3 must be linked to the α primary precipitation process, although it can also have a contribution from different out of equilibrium processes like structural recovery or vacancies annihilation. According to the high temperature exothermic peak, the decomposition process $\gamma \rightarrow \alpha+\gamma_1$ should be completed only well above 973 K.

In order to explore the influence of both precipitation processes on the mechanical properties and on the MT characteristics, Fig. 6 shows the temperature dependence of the damping (a) and modulus (b) measured in warming during thermal cycles performed up to different maximum temperatures which are increased in steps of 20 K. Fig. 6a also shows the damping after an *in situ* isothermal annealing at 773 K during three hours.

The peak height related to the MT exhibits a non-monotonous change with the annealing temperature, see Fig. 6a. Moreover, the MT peak is almost absent for the annealed sample at 773 K during 3 h. In addition, P_1 peak decreases after the first heating up to 603 K due to the recovery of the structure and it keeps a similar shape during the further successive thermal cycles; in agreement with previous works [39,41].

The moduli in Fig. 6b exhibit the change related to the MT at around 320 K and the inverse dependence on temperature related to the dragging of defects at higher temperatures. The modulus increase during the successive thermal cycles can be related to the recovery of the structure and to the precipitation processes, in agreement with XRD, ND, ADD and DSC results. It is interesting to note that the

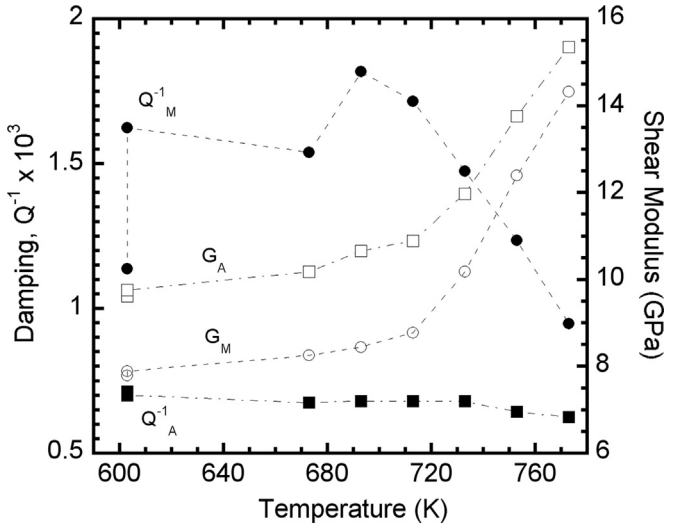

Fig. 7. Damping (Q^{-1}, full symbols) and modulus (G, empty symbols) for the austenitic and martensitic phases as a function of the maximum temperature achieved in the previous thermal MS cycle. Values for the austenitic (sub index A) and martenstitic (sub index M) phases were evaluated at 370 K and 280 K, respectively. Lines are a guide for the eyes.

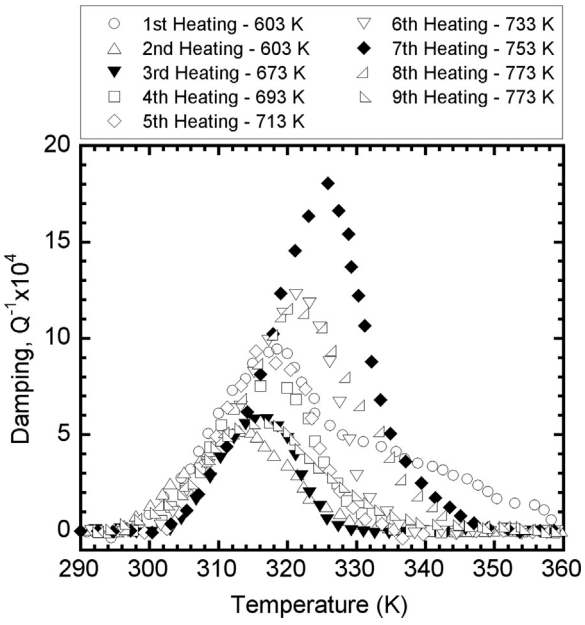

Fig. 8. Damping peaks related to the martensitic transformation corresponding to spectra from Fig. 6a after the background subtraction.

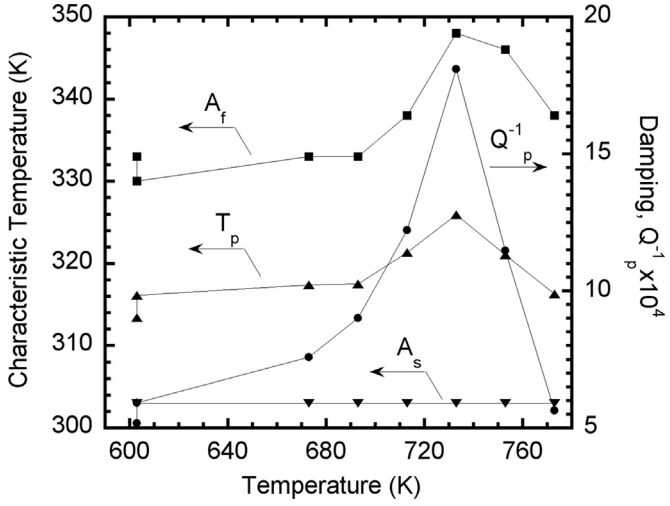

Fig. 9. Peak temperature of the damping peak related to the martensitic transformation (Tp, triangles), austenite finish temperature (A_f, squares), austenite start temperature (A_s, inverted triangles) and peak height of the damping peak related to the martensitic transformation (Q^{-1}_p, circles), as a function of the maximum temperature achieved in the previous thermal MS cycle. Lines are a guide for the eyes.

modulus curve for the sample annealed at 773 K during three hours exhibit a usual dependence on temperature, in agreement with highly developed precipitation and recovery processes.

Fig. 7 shows the behaviour of the modulus and damping as a function of the maximum annealing temperature achieved in the previous thermal cycle. Moduli (empty symbols) and damping values (full symbols) for the martensite at 280 K (circles) and austenite at 370 K (squares), are shown in the figure.

It should be highlighted the appearance of an age–hardening behaviour during the thermal cycles which leads to an increase in the modulus for the martensite and austenite phases in around 60% and 45%, respectively. Indeed, the hardening mechanism is controlled by the precipitation of small particles of α phase. Moreover, the hardening after a thermal cycle up to 1000 K leads to an increase in the modulus of around 90%, but it deteriorate completely the MT as a consequence of the decomposition of the metastable γ phase into the $\alpha+\gamma_1$. In addition, for the austenite phase the hardening is achieved without a marked detriment in the damping capacity independently of the final temperature of the thermal cycle, see Figs. 1 and 7.

Regarding to the effect of thermal cycles on the MT, Fig. 8 shows the MT damping peaks after the background subtraction. It can be observed that both the MT peak temperature (T_p) and the damping peak height ($Q^{-1}{}_p$) increase after the second warming up to 603 K. In contrast, after the first warming up to 773 K the peak height decreases markedly and the peak temperature shifts towards smaller temperatures. In order to analyze carefully this evolution, Fig. 9 shows the peak temperature and the peak height as a function of the maximum annealing temperature achieved in the previous thermal cycle. In fact, the first annealing at 603 K leads to a reduction of the damping height and the peak temperature due to the relaxation of the internal stresses promoted by the recovery of the quenched-in-defects; in agreement with previous works [39,41]. In contrast, thermal cycles performed between 603 K and 753 K (runs #2 to #7 in Figs. 8 and 9) lead to an increase in the peak height (twice) which can be controlled by the precipitation of the α phase. Indeed, the appearance of small precipitates of α phase could increase the contribution to the damping due to the larger amount of defects to be dragged during the movement of variants [41] and the development of MT. The shift of the peak temperature towards higher temperatures is related to the widening of the damping peak promoted by the progressive increase in the austenite finish (A_f) value, see Fig. 9. On the contrary, as shown in Fig. 8, the start of the transformation (A_s, austenite start) is slightly modified, which is revealed by the overlapping of the low temperature tails of the peaks in the figure.

The increase in A_f can be explained considering the precipitation process of the α phase. Indeed, the precipitation of α phase involves small both precipitates and volume fractions, so the composition of the matrix is slightly modified. In addition, the appearance of α precipitates at nanometric scale increases the elastic contribution to the MT and requires more thermal energy to develop the reverse transformation.

It should be stressed that thermal treatments performed at low temperatures modify the MT characteristics giving rise to adaptable properties that can be tuned depending on the particular technological requirements.

In contrast, higher annealing temperatures (above 753 K) produce a decrease in the MT temperature due to the decomposition process $\alpha+\gamma_1$. Apart from the defects recovery that can change the relative

stability between martensite and austenite, the chemical energy changes dominate the MT kinetics due to composition changes in the matrix. The significant increase in the amount of α precipitates depletes the γ matrix of iron, shifting the transformation to lower temperatures and creating composition gradients. In fact, an increase in the amount of α precipitates leads to a decrease in the transformed volume fraction and can also inhibit completely the MT, after annealing treatments above 1000 K, see Fig. 1a. Then, the precipitation of the phases $\alpha+\gamma_1$ modify the main characteristics of MT limiting the application at elevated temperatures of this alloy.

4. Conclusions

Mechanical spectroscopy allows determining the influence of thermal treatments on both, the hardening and damping behaviours and the main characteristics of the martensitic transformation in a $Fe_{66.8}Pd_{30.7}Mn_{2.5}$ alloy.

Annealing below 753 K leads to: (i) a hardening in the austenitic and martensitic phases of around 35% and 45%, respectively. (ii) a decrease in the damping capacity of the alloy in austenite phase less than 10%. However, the decrease in damping capacity in the martensitic phase is around 28%. (iii) an increase in both the austenite finish transformation temperature and in the intensity of the damping peak related to the martensitic transformation. This change is controlled by the precipitation of small precipitates and small volume fractions of the α phase. Therefore, thermal treatments performed at low temperatures can be used to adapt the properties of the alloy depending on the technological requirements. In contrast, thermal treatments performed above 753 K decrease the austenitic finish transformation temperature and the intensity of the damping peak related to the martensitic transformation. The change is now controlled by the decomposition of the metastable γ phase into the $\alpha+\gamma_1$ stable phases. Moreover, long annealing above 773 K or thermal cycles up to 1000 K lead to a hardening of around 90%, but they reduce markedly the development of the martensitic transformation.

Furthermore, two new relaxation peaks, called P_2 and P_3, have been discovered at around 700 K and 900 K, respectively. The P_2 peak could be related to a process into which the vacancies are created and dragged by a dislocation movement. On the other side, the P_3 peak is related to the grain boundary mobility phenomenon and it can be related to the solute grain boundary peak of palladium in iron.

Acknowledgment

This work has been carried out with the financial support of the Spanish "Ministerio de Economía y Competitividad" (Project number MAT2015-65165-C2-R), the CONICET-PIP 0179, and the PID-UNR; ING 453 (2014–2017). The Institut Laue-Langevin, D20 installation (Grenoble, France), is acknowledged for the allocated neutron beam-time (Exp. 1-01-129). Authors also wish to acknowledge to the Cooperation Agreement between the Universidad Pública de Navarra and the Universidad Nacional de Rosario, Res. 3247/2015, and the Cooperation Agreement between the Universidad del País Vasco/ Euskal Herriko Unibertsitatea and the Universidad Nacional de Rosario, Res 3243/2015. A.O.L wishes to say thanks to his friend the Rev. P. Ignacio Peries for everything.

References

[1] R. Oshima, Successive martensitic transformations in Fe-Pd alloys, Scr. Met. 15 (1981) 829–833.
[2] R. Oshima, M. Sugiyama, Martensite transformations in Fe-Pd alloys, J. Phys. IV 43 (1982) C4–383.
[3] M. Sugiyama, R. Oshima, F.E. Fujita, Martensitic transformation in the Fe–Pd alloy system, Trans. JIM 19 (1984) 585–592.
[4] M. Sugiyama, S. Harada, R. Oshima, Change in young's modulus of thermoelastic martensite Fe-Pd alloys, Scr. Met. 19 (1985) 315–317.
[5] M. Sugiyama, R. Oshima, F.E. Fujita, Mechanism of FCC-FCT thermoelastic martensite transformation in Fe–Pd alloys, Trans. JIM 27 (1986) 719–730.
[6] S. Muto, R. Oshima, F.E. Fujita, Relation of magnetic domain structure to FCT martensite variants in Fe-Pd alloys, Scr. Met. 21 (1987) 465–468.
[7] R. Oshima, M. Sugiyama, F.E. Fujita, Tweed structures associated with fcc-fct transformations in Fe-Pd alloys, Metall. Trans. A 19 (1988) 803–810.
[8] S. Muto, S. Takeda, R. Oshima, F.E. Fujita, High-resolution electron microscopy of the tweed microstructure in an Fe-Pd alloy, Jpn. J. Appl. Phys. 27 (1988) L1387.
[9] S. Muto, R. Oshima, F.E. Fujita, Consideration of the tweed structure of Fe-Pd alloys by continuum elasticity theory, Mater. Sci. Forum 56 (1990) 65–70.
[10] S. Muto, S. Takeda, R. Oshima, Analysis of lattice modulations in the tweed structure of an Fe–Pd alloy by image processing of a high-resolution electron micrograph, Jpn. J. Appl. Phys. 29 (1990) 2066.
[11] K. Tanaka, R. Oshima, Role of annealing twin in the formation of variant structure of bct martensite in Fe–Pd alloy, Mater. Trans. JIM 32 (1991) 325–330.
[12] R. Oshima, S. Muto, F.E. Fujita, Initiation of FCC-FCT thermoelastic martensite transformation from premartensitic state of Fe-30 at% Pd alloys, Mater. Trans. JIM 33 (1992) 197–202.
[13] J. Cui, T.W. Shield, R.D. James, Phase transformation and magnetic anisotropy of an iron–palladium ferromagnetic shape-memory alloy, Acta Mater. 52 (2004) 35–47.
[14] R.A. Stern, S.D. Wiiloughby, A. Ramirez, J.M. Maclaren, J. Cui, Q. Pan, R.D. James, Electronic and structural properties of Fe_3Pd-Pt ferromagnetic shape memory alloys, J. Appl. Phys. 91 (2002) 7818–7820.
[15] K. Tanaka, K. Hiraga, R. Oshima, Origin of tetragonality of BCT martensite in substitutional Fe–Pd (–Ni) disordered alloys, Mater. Trans. JIM 33 (1992) 215–219.
[16] K. Tsuchiya, T. Nojiri, H. Ohtsuka, M. Umemoto, Effect of Co and Ni on martensitic transformation and magnetic properties in Fe-Pd ferromagnetic shape memory alloys, Mater. Trans. JIM 44 (2003) 2499–2502.
[17] T. Wada, T. Tagawa, M. Taya, Martensitic transformation in Pd-rich Fe–Pd–Pt alloy, Scr. Mater. 48 (2003) 207–211.
[18] D. Vokoun, Y.W. Wang, T. Goryczka, C.T. Hu, Magnetostrictive and shape memory properties of Fe–Pd alloys with Co and Pt additions, Smart Mat. Struct. 14 (2005) S261.
[19] Y.C. Lin, H.T. Lee, S.U. Jen, Y.T. Chen, Magnetic structure of an Fe–Pd–Rh alloy, J. Appl. Phys. 101 (2007) 09N514.
[20] S.U. Jen, Y.T. Chen, T.L. Tsai, Y.C. Lin, Magnetostrictive strains in polycrystalline FePdRh alloy, J. Appl. Phys. 103 (2008) 07B902.
[21] V. Sánchez-Alarcos, V. Recarte, J.I. Pérez-Landazábal, C. Gómez-Polo, V.A. Chernenko, M.A. González, Reversible and irreversible martensitic transformations in Fe-Pd and Fe-Pd-Co alloys, Eur. Phys. J. Spec. Top. 158 (2008) 107–112.
[22] V. Sánchez-Alarcos, J.I. Pérez-Landazábal, V. Recarte, Effect of Co and Mn doping on the martensitic transformations and magnetic properties of Fe-Pd ferromagnetic shape memory alloys, Mater. Sci. Forum 635 (2010) 103–110.
[23] V. Sánchez-Alarcos, V. Recarte, J.I. Pérez-Landazábal, M.A. González, J.A. Rodríguez-Velamazan, Effect of Mn addition on the structural and magnetic properties of Fe–Pd ferromagnetic shape memory alloys, Acta Mater. 57 (2009) 4224–4232.
[24] M. Hansen, K. Anderko, Constitution of Binary Alloys, McGraw-Hill Inc, New York, 1985.
[25] M.E. Gruner, P. Entel, Impact of local lattice distortions on the structural stability of Fe-Pd magnetic shape-memory alloys, Phys. Rev. B 83 (2011) 214415.
[26] I. Claussen, R.A. Brand, H. Hahn, S.G. Mayr, Relaxation scenarios in Fe–Pd and Fe–Pd–Cu ferromagnetic shape memory splats: short range order and microstructure, Scr. Mater. 66 (2012) 163–166.
[27] J.K. Lee, Y.Y. Earmme, H.I. Aaronson, K. Russell, Plastic relaxation of the transformation strain energy of a misfitting spherical precipitate: ideal plastic behavior, Metal. Trans. A 11 (1980) 1837–1847.
[28] T. Mura, Micromechanics of Defects in Solids, Martinus Nijhoff Publishers, New York, 1987.
[29] M. Shibata, K. Ono, The strain energy of a spheroidal inclusion and its application to bcc-hcp martensitic transformation, Acta Metal. 2 (1975) 587–597.
[30] M. Shibata, K. Ono, On the minimization of strain energy in the martensitic transformation of titanium, Acta Metal. 25 (1977) 35–42.
[31] E. Patoor, D.C. Lagoudas, P.B. Entchev, L. Catherine Brinson, X. Gao, Shape memory alloys, Part I: general properties and modeling of single crystals, Mech. Mater. 38 (2006) 391–429.
[32] D.C. Lagoudas, P.B. Entchev, P. Popov, E. Patoor, L. Catherine Brinson, X. Gao, Shape memory alloys, Part II: modeling of polycrystals, Mech. Mater. 38 (2006) 430–462.
[33] J. Buschbeck, I. Opahle, M. Richter, U.K. Röbler, P. Klaer, M. Kallmayer, H.J. Elmers, G. Jakob, L. Schultz, S. Fähler, Full tunability of strain along the fcc-bcc Bain path in epitaxial films and consequences for magnetic properties, Phys. Rev. Lett. 103 (2009) 216101.
[34] A. Budruk, C. Phatak, A.K. Petford-Long, M. De Graef, In situ Lorentz TEM magnetization studies on a Fe–Pd–Co martensitic alloy, Acta Mater. 59 (2011) 6646–6657.
[35] R. Schaller, G. Fantozzi, G. Gremaud (Eds.), Mechanical Spectroscopy, Trans Tech Publications, Zurich, 2001.
[36] A.S. Nowick, B.S. Berry, Anelastic Relaxation in Crystalline Solids, Academic Press, New York, 1972.
[37] C. Zener, Elasticity and Anelasticity of Metals, University of Chicago Press, Chicago, 1956.
[38] O.A. Lambri, A review on the problem of measuring nonlinear damping and the

obtainment of intrinsic damping, in: J. Martinez-Mardones, D. Walgraef, C.H. Wörner (Eds.), Materials Instabilities, World Scientific Publishing, New York, 2000.
[39] J.I. Pérez-Landazábal, O.A. Lambri, F.G. Bonifacich, V. Sánchez-Alarcos, V. Recarte, F. Tarditti, Influence of defects on the irreversible phase transition in Fe–Pd ferromagnetic shape memory alloys, Acta Mater. 86 (2015) 110–117.
[40] F. Xiao, T. Fukuda, T. Kakeshita, M. Jin, X. Jin, Dynamic mechanical analysis of weak first-order martensitic transformation in an iron–palladium alloy, J. Alloy. Compd. 649 (2015) 211–215.
[41] F.G. Bonifacich, O.A. Lambri, J.I. Pérez-Landazábal, D. Gargicevich, V. Recarte, V. Sánchez-Alarcos, Mobility of twin boundaries in Fe-Pd ferromagnetic shape memory alloys, Mater. Trans. JIM 57 (2016) 1837–1844.
[42] C. Seguí, E. Cesari, J. Pons, V.A. Chernenko, Internal friction behaviour of Ni-Mn-Ga, Mat. Sci. Eng. A 370 (2004) 481–484.
[43] J. Van Humbeeck, Damping capacity of thermoelastic martensite in shape memory alloys, J. Alloy. Comp. 355 (2003) 58–64.
[44] B.J. Molinas, O.A. Lambri, M. Weller, Study of non-linear effects related to the Snoek-Köster relaxation in Nb, J. Alloy. Compd. 211–212 (1994) 181–184.
[45] G.I. Zelada-Lambri, O.A. Lambri, J.A. García, Mechanical energy losses due to the movement of dislocations in molybdenum at high temperatures (0.3T m), J. Nucl. Mater. 353 (2006) 127–134.
[46] Peak Fit, V. 4, Jandel Scientific Software, Germany, 1995.
[47] J. Friedel, Dislocations, Addison-Wesley, Reading, 1967.
[48] F. Mezzetti, L. Passari, D. Nobili, Study of relaxation peaks in austenitic steels, in: Proceedings of the Fifth International Conference on Internal Friction and Ultrasonic Attenuation in Solids, vol. I, Aachen, Germany, 1973, pp. 436–443.
[49] S.A. Golovin, K. Belkin, Damping capacity in plastically deformed austenitic steels, Fiz. Metal. Met. 20 (1965) 763–769.
[50] G.I. Zelada-Lambri, O.A. Lambri, G.H. Rubiolo, Amplitude dependent damping study in austenitic stainless steels 316 H and 304 H, Its relation with the microstructure, J. Nucl. Mat. 273 (1999) 248–256.
[51] G. Schoeck, Fricción interna debido a la interacción entre dislocaciones y átomos solutos, Acta Metall. 11 (1963) 617–622.
[52] T.L. Wu, C.M. Wang, Mechanism of carbon diffusion peak in fcc iron-nickel alloys, Acta Phys. Sin. 14 (1958) 354–368.
[53] V.D. Verner, Nature of the internal friction peak in face centered cubic interstitial solid solutions, Sov. Phys. Solid State 7 (1966) 1874–1880.
[54] M. Weller, M. Tietze, J. Diehl, A. Seeger, The Snoek-Koester relaxation in body-centered cubic metals, in: V. Paidar, L. Lejeck (Eds.), The Structure and Properties of Crystal Defects, Materials Science Monographs, Elsevier, Amsterdam, 1984, pp. 215–222.
[55] O.A. Lambri, G.I. Zelada-Lambri, L.M. Salvatierra, J.A. García, J.N. Lomer, Anelastic relaxation in high purity molybdenum single crystals at medium temperatures, Mat. Sci. Eng. A 370 (2004) 222–224.
[56] M. Eldrup, Application of the positron annihilation technique in studies of defects in solids, in: A.V. Chadwick, M. Terenzi (Eds.), NATO ASI Series, Plenum, New York, 1985, p. 145.
[57] O.A. Lambri, J.I. Pérez-Landazábal, J.A. Cano, V. Recarte, Mechanical spectroscopy in commercial Fe–6 wt% Si alloys between 400 and 1000 K, Mat. Sci. Eng. A 370 (2004) 459–463.
[58] J. Philibert, Atom movements: Diffusion and Mass Transport in Solids (Monographies de Physique), Les editions de Physique, Les Ulis Cedex A, 1991.
[59] M. Koiwa, Diffusion in materials – history and recent developments, Mater. Trans. JIM 39 (1988) 1169–1179.
[60] G.I. Zelada-Lambri, O.A. Lambri, P.B. Bozzano, J.A. García, C.A. Celauro, Interaction processes between vacancies and dislocations in molybdenum in the temperature range around 0.3 of the melting temperature, J. Nucl. Mat. 380 (2008) 111–119.
[61] E.A. Brandes, G.B. Brook, P. Paufler (Eds.), Smithells Metals Reference Book, Butterworth-Heinemann Ltd., Oxford, 1993.
[62] B.S. Bokshtein, Difusión en Metales, MIR, Moscú, 1980.
[63] G.I. Zelada, O.A. Lambri, P.B. Bozzano, J.A. García, Mechanical energy losses in plastically deformed and electron plus neutron irradiated high purity single crystalline molybdenum at elevated temperatures, Phys. Status Solidi A 209 (2012) 1972–1977.
[64] F. Povolo, B.J. Molinas, Present state of the controversy about the grain boundary relaxation, Nuovo Cimento D 14 (1992) 287–332.
[65] O.A. Lambri, W. Riehemann, Z. Trojanová, Mechanical spectroscopy of commercial AZ91 magnesium alloy, Scr. Mater. 45 (2001) 1365–1371.
[66] O.A. Lambri, W. Riehemann, L.M. Salvatierra, J.A. García, Effects of precipitation processes on damping and elastic modulus of WE 43 magnesium alloy, Mater. Sci. Eng. A 373 (2004) 146–157.
[67] D.R. Mosher, R. Raj, Use of the internal friction technique to measure rates of grain boundary sliding, Acta Metall. 22 (1974) 1469–1474.
[68] R. De Batist, Mechanical spectroscopy, in: E. Lifshitz (Ed.), Characterization of Materials, in: R.W. Cahn, P. Haasen, E.J. Kramer (Eds.), Materials Science and Technology, vol. 2B, Part II, VCH, Weinheim, 1991.
[69] T.B. Massalski, Binary Alloy Phase Diagrams, ASM International, Materials Park, Ohio, 1996.
[70] K. Watanabe, Isothermal heat-treatment and phase transformation of Fe-Pd permanent magnet alloys, T. Jpn. Inst. Met. 24 (1983) 144–148.